ISSN 2035-911X

International Journal of
Energy & Technology
www.journal-enertech.eu

International Journal of Energy & Technology 5 (9) (2013) 1–13

EFFECT OF HEATING WALL POSITION ON FORCED CONVECTION ALONG TWO SIDED OPEN ENCLOSURE WITH POROUS MEDIUM UTILIZING NANOFLUID

Rehena Nasrin[*, 1], M.A. Alim[1] and Ali J. Chamkha[2]

[1]Department of Mathematics, Bangladesh University of Engineering and Technology, Dhaka - 1000, Bangladesh, *E-mail: rehena@math.buet.ac.bd

[2]Manufacturing Engineering Department, The Public Authority for Applied Education and Training, Shuweikh 70654, Kuwait

ABSTRACT

Forced convection in a channel with an open cavity having porous medium is studied numerically. A uniform heat flux is considered to be located along left, bottom and right walls of the open cavity. Three basic heating modes are considered: (a) the heated wall is on the inflow side (assisting flow); (b) the heated wall is on the outflow side (opposing flow) and (c) the heated wall is the horizontal surface of the cavity (heating from below). The rest of the surfaces are taken to be perfectly insulated. The physical domain is filled with water based nanofluid containing titanium oxide (TiO_2) naparticles. The fluid enters from left and exits from right with initial velocity U_i and temperature T_i. Governing equations are discretized using the Finite Element Method. Forced convection fluid flow and heat transfer within the cavity is governed by the inertia force and viscosity parameter namely Reynolds number (*Re*) and Prandtl number (*Pr*). The simulation is carried out for a wide range of Reynolds number *Re* (= 10-300) and solid volume fraction ϕ (= 0% - 7%). Results are presented in the form of streamlines, isothermal lines, local and average Nusselt number, average temperature of the fluid and horizontal and vertical velocities at mid-height of the channel for various *Re* and ϕ. The enhancement of heat transfer rate is caused by increasing both *Re* and ϕ. The present investigation shows that the opposing forced flow configuration has the highest thermal performance in terms of both maximum temperature of the nanofluid and average Nusselt number.

Keywords: Water-TiO_2 nanofluid, forced convection, channel with open cavity, porous medium, finite element method.

1. INTRODUCTION

Nanofluid is made by adding nanoparticles and a surfactant into a base fluid can greatly enhance thermal conductivity and convective heat transfer. The diameters of nanoparticles are usually less than 100 nm which improves their suspension properties. Nanofluid technology has emerged as a new enhanced heat transfer technique in recent years. The knowledge of forced convection heat transfer inside geometries of irregular shape (for example, channel, pipe bend, channel with cavity) for porous media has many significant engineering applications; for example, geothermal engineering, solar-collectors, performance of cold storage, and thermal insulation of buildings.

The deal with flow characteristics, heat transfer, flow and heat transfer instability, transition to turbulence, design aspects, etc is available in some published articles. Many researchers [1–5] considered different physical situations which can be classified into two broad groups. The first group problems cover a wide range of applications; for example, flow through blood vessels, food industries, large industrial heat exchangers, etc. In contrast, the relatively new second group deals with the natural convection problem in an enclosed space with wavy walls. Starting from the microelectronic heat transfer cooling device this group covers a wide range of significant engineering applications; for example, microelectro- mechanical device, double-wall thermal insulation, underground cable systems, solar-collectors, electric machinery, etc. Significant contributions have been made by several researchers [6–8] in order to model the problems of this specific group. For wavy cavities filled with porous medium that obeys the Darcy law, Kumar [9] reported flow and heat transfer results in a cavity with wavy bottom wall. This work is extended for one vertical wavy surface in Kumar and Gupta [10-11]. They reported the flow and thermal fields' characteristics in wavy cavities for non-Darcy porous medium.

Misirlioglu et al. [12] was analyzed free convection in a wavy cavity filled with a porous medium. Santra et al. [13] modeled the nanofluids as a non-Newtonian fluid and observed a systematic decrease of the heat transfer as the volume fraction of the nanofluids increased. Kumar et al. [14] found the significant heat transfer enhancement by the dispersion of nanoparticles in the base fluid. The possible determining factors for the heat transfer reduction in nanofluids include the variations of the size, shape, and distribution of nanoparticles and uncertainties in the thermophysical properties of nanofluids.

The analysis of natural convection heat transfer of nanofluids in square or rectangular enclosures is considered by most of the published papers; for example, Ghasemi and Aminossadati [15], Abu-Nada and Oztop [16], Muthtamilselvan et al. [17] and Abu-Nada et al. [18]. In reality forced convection in a differentially heated enclosure is a prototype of many industrial applications and has received considerable attention because of its applicability in various fields. The study of convective flow in a complicated geometry is more difficult than that of square or rectangular enclosures. Many studies have described the larruping behaviors of nanofluids, such as their effective thermal conductivity under static conditions on the convective heat transfer associated with fluid flow phenomena. Chen et al. [19] and Dai et al. [20] investigated convective flow drag and heat transfer of CuO nanofluid in a small tube. Their results showed that the pressure drop of the nanofluid per unit length was greater than that of water. The pressure drop increased with the increasing weight concentration of nanoparticles. In the laminar flow region, the pressure drop had a linear relationship with the *Re* number, while in the turbulent flow region, the pressure drop increased sharply with the increase of the *Re* number. The critical *Re* number became lower while the tube diameter was smaller.

By adding nanoparticles the convective heat transfer is obviously enhanced. The nanoparticle weight concentration and flow status are the main factors influencing the heat transfer coefficient: the heat transfer coefficient increases with the increasing weight concentration, and the enhancement of heat transfer in the turbulent flow region is generally greater than that in the laminar flow region. Pfautsch [21] studied the characteristics, flow development and heat transfer coefficient of nanofluids under laminar forced convection over a flat plate. He found a significant increase in the heat transfer coefficient: about 16% increase in the heat transfer coefficient for the water based nanofluid and about 100% increase for the ethylene glycol based nanofluid. Recently, Nasrin et al. [22] studied non-darcy forced convection through a wavy channel using CuO nanofluid. They found that the rate of heat transfer in the channel was increased for both *Re* and ϕ but it was lessened for higher *Da*. Forced convection in a channel with transverse fins was analyzed by Yang et al. [23] where the optimum aspect ratio of a fin increased with Reynolds number and fin spacing but decreased with thermal conductivity ratio and entrance length with other parameters fixed.

Transient analysis on forced convection phenomena in a fluid valve was conducted by Nasrin et al. [24]. The result showed that the rate of heat transfer in the fluid valve reduced for longer time periods. Sathiyamoorthy and Chamkha [25] conducted natural convection flow under magnetic field in a square cavity for uniformly heated walls. It was found that the presence of a magnetic filed caused significant effects on the local and average Nusselt numbers on all considered walls.

Very recently, Nasrin et al. [26-31] modeled of mixed, free and forced convective heat transfer utilizing nanofluid through various geometries. They used finite element method for solving the governing partial differential equations. Mixed convection in an inclined channel with heated porous blocks was investigated by Guerroudj and Kahalerras [32]. Their results revealed that the inclination angle of the channel could alter substantially the fluid flow and heat transfer mechanisms, especially at high Richardson and Darcy numbers.

So far, there is no research on the analysis of forced convective heat transfer with porous medium using nanofluid in a channel. Therefore, forced convection also becomes a crucial point of this study. The main issues discussed in this paper are: the convective flow and heat transfer characteristics of water-TiO_2 nanofluid in a horizontal channel with an open cavity.

2. PHYSICAL CONFIGURATION

Fig. 1 shows a schematic diagram of the horizontal channel with an open cavity. The model describes a channel with two insulated walls. Flow enters from left and leaves from the right. The open cavity lies at the lower wall of the channel. Three basic heating modes are considered: (a) the heated wall is on the inflow side (assisting flow); (b) the heated wall is on the outflow side (opposing flow); and (c) the heated wall is the horizontal surface of the cavity (heating from below). These walls are heated by a uniform heat flux. The inlet fluid velocity and temperature are U_i and T_i respectively. The working fluid through the channel with open cavity is water-TiO_2 nanofluid.

3. MATHEMATICAL FORMULATION

In the present problem, it is considered that the flow is steady, two-dimensional, laminar, incompressible and there is no viscous dissipation**.** The radiation effect is neglected. The governing equations under Boussinesq approximation are as follows

$$\frac{\partial u}{\partial x}+\frac{\partial v}{\partial y}=0 \tag{1}$$

$$\rho_{nf}\left(u\frac{\partial u}{\partial x}+v\frac{\partial u}{\partial y}\right)=-\frac{\partial p}{\partial x}+\mu_{nf}\left(\frac{\partial^2 u}{\partial x^2}+\frac{\partial^2 u}{\partial y^2}\right)-\frac{\mu_{nf}}{K}u \tag{2}$$

$$\rho_{nf}\left(u\frac{\partial v}{\partial x}+v\frac{\partial v}{\partial y}\right)=-\frac{\partial p}{\partial y}+\mu_{nf}\left(\frac{\partial^2 v}{\partial x^2}+\frac{\partial^2 v}{\partial y^2}\right)-\frac{\mu_{nf}}{K}v \tag{3}$$

$$u\frac{\partial T}{\partial x}+v\frac{\partial T}{\partial y}=\alpha_{nf}\left(\frac{\partial^2 T}{\partial x^2}+\frac{\partial^2 T}{\partial y^2}\right) \tag{4}$$

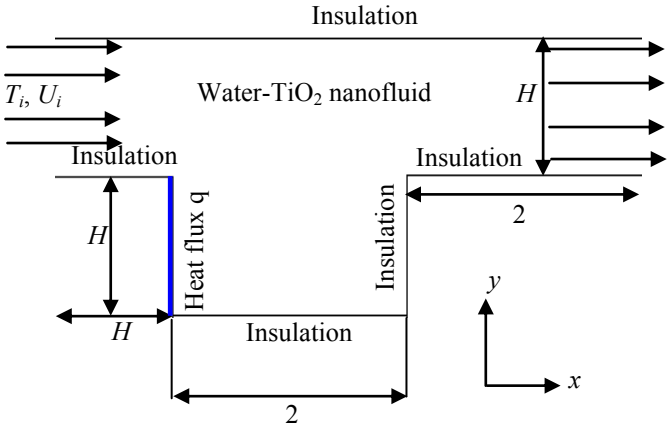

1(a)

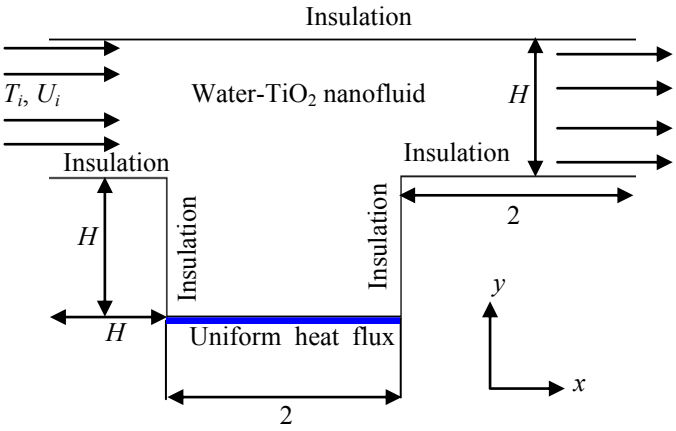

1(b)

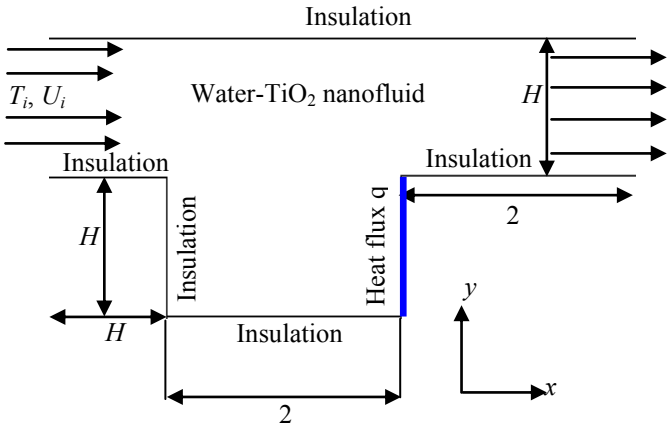

1(c)

Fig. 1: Depiction of the geometry and the operation of the channel with an open cavity (a) assisting flow, (b) heating from below and (c) opposing flow

where, $\rho_{nf} = (1-\phi)\rho_f + \phi\rho_s$ is the density,

$(\rho C_p)_{nf} = (1-\phi)(\rho C_p)_f + \phi(\rho C_p)_s$ is the heat capacitance,

$\beta_{nf} = (1-\phi)\beta_f + \phi\beta_s$ is the thermal expansion coefficient,

$\alpha_{nf} = k_{nf} / (\rho C_p)_{nf}$ is the thermal diffusivity,

In the current study, the viscosity of the nanofluid is considered by the Pak and Cho correlation [33]. This correlation is given as

$$\mu_{nf} = \mu_f \left(1 + 39.11\phi + 533.9\phi^2\right) \tag{5}$$

The effective thermal conductivity of the nanofluid is approximated by the Maxwell-Garnett model [34]:

$$\frac{k_{nf}}{k_f} = \frac{k_s + 2k_f - 2\phi(k_f - k_s)}{k_s + 2k_f + \phi(k_f - k_s)} \tag{6}$$

The non-dimensional boundary conditions are:

at the inlet: $T = T_i$, $u = U_i$

at the outlet: convective boundary condition $p = 0$

at all solid boundaries : $u = v = 0$

at all solid boundaries of the channel: $\frac{\partial T}{\partial y} = 0$

and a uniform heat flux q is considered at the left, bottom and right boundaries of the cavity in Fig 1(a), (b) and (c) respectively. Other boundaries of the cavity are perfectly insulated.

The above equations are non-dimensionalized by using the following dimensionless dependent and independent variables

$$X = \frac{x}{H},\ Y = \frac{y}{H},\ U = \frac{u}{U_i},\ V = \frac{v}{U_i},\ P = \frac{p}{\rho_f U_i^2},\ \theta = \frac{(T - T_i)k_f}{qH}$$

After substitution of the above variables into the equations (1) to (4), we get the following non-dimensional equations as

$$\frac{\partial U}{\partial X} + \frac{\partial V}{\partial Y} = 0 \tag{7}$$

$$U\frac{\partial U}{\partial X} + V\frac{\partial U}{\partial Y} = -\frac{\rho_f}{\rho_{nf}}\frac{\partial P}{\partial X} + Pr\frac{\nu_{nf}}{\nu_f}\left(\frac{\partial^2 U}{\partial X^2} + \frac{\partial^2 U}{\partial Y^2}\right) - \frac{\nu_{nf}}{Da}U \tag{8}$$

$$U\frac{\partial V}{\partial X} + V\frac{\partial V}{\partial Y} = -\frac{\rho_f}{\rho_{nf}}\frac{\partial P}{\partial Y} + Pr\frac{\nu_{nf}}{\nu_f}\left(\frac{\partial^2 V}{\partial X^2} + \frac{\partial^2 V}{\partial Y^2}\right) - \frac{\nu_{nf}}{Da}V \tag{9}$$

$$U\frac{\partial \theta}{\partial X} + V\frac{\partial \theta}{\partial Y} = \frac{1}{Re\,Pr}\left(\frac{\partial^2 \theta}{\partial X^2} + \frac{\partial^2 \theta}{\partial Y^2}\right) \tag{10}$$

where $Pr = \frac{\nu_f}{\alpha_f}$ is Prandtl number, $Re = \frac{U_i H}{\nu_f}$ is Reynolds number and $Da = \frac{K}{H^2}$ is Darcy number.

The corresponding boundary conditions then take the following form:

at the inlet: $\theta = 0$, $U = 1$

at the outlet: convective boundary condition $P = 0$

at all solid boundaries: $U = V = 0$

at all solid boundaries of the channel: $\dfrac{\partial \theta}{\partial Y} = 0$

and at the left, bottom and right boundaries of the cavity are maintained non-dimensional uniform heat flux condition in Fig. 1(a), (b) and (c) respectively. Other walls of the cavity are insulated.

The local and average Nusselt numbers at the left and right vertical heated surfaces of the enclosure may be expressed, respectively as

$$Nu_{local} = -\left(\frac{k_{nf}}{k_f}\right)\frac{\partial \theta}{\partial X} \quad \text{and} \quad Nu = -\frac{1}{L}\int_0^L \left(\frac{k_{nf}}{k_f}\right)\frac{\partial \theta}{\partial X} dY .$$

Similarly, for the bottom heated surface of the enclosure the formula may be expressed, respectively as

$$Nu_{local} = -\left(\frac{k_{nf}}{k_f}\right)\frac{\partial \theta}{\partial Y} \quad \text{and} \quad Nu = -\frac{1}{L}\int_0^L \left(\frac{k_{nf}}{k_f}\right)\frac{\partial \theta}{\partial Y} dX$$

where L is the dimensionless length of the heated surface.

For convenience, a normalized average Nusselt number is defined as the ratio of the average Nusselt number at any volume fraction of nanoparticles to that of the pure water, which is:

$$Nu^*(\phi) = \frac{Nu(\phi)}{Nu(\phi = 0)}$$

The mean bulk temperature of the fluid inside the enclosure may be written as $\theta_{av} = \int \theta \, d\bar{V} / \bar{V}$ where $\bar{V}$ is the volume of the channel having an open cavity.

4. NUMERICAL TECHNIQUE

The Galerkin finite element method [35, 36] is used to solve the non-dimensional governing equations along with boundary conditions for the considered problem. The equation of continuity has been used as a constraint due to mass conservation and this restriction may be used to find the pressure distribution. The finite element method is used to solve Eqs. (8) - (10), where the pressure P is eliminated by a penalty constraint ξ, and the incompressibility criteria given by Equation (7) which can be expressed as

$$P = -\xi\left(\frac{\partial U}{\partial X} + \frac{\partial V}{\partial Y}\right) \tag{11}$$

The continuity equation is automatically fulfilled for large values of ξ. Then the velocity components (U, V), and temperature (θ) are expanded using a basis set $\{\Phi\}_{k=1}^{N}$ as

$$U \approx \sum_{k=1}^{N} U_k \Phi_k(X,Y), \qquad V \approx \sum_{k=1}^{N} V_k \Phi_k(X,Y) \qquad \text{and}$$

$$\theta \approx \sum_{k=1}^{N} \theta_k \Phi_k(X,Y) \tag{12}$$

The Galerkin finite element technique yields the subsequent nonlinear residual equations for the Eqs. (8), (9) and (10) respectively at nodes of the internal domain Ω

$$\begin{aligned} R_i^{(1)} &= \sum_{k=1}^{N} U_k \int_\Omega \left[\left(\sum_{k=1}^{N} U_k \Phi_k\right)\frac{\partial \Phi_k}{\partial X} + \left(\sum_{k=1}^{N} V_k \Phi_k\right)\frac{\partial \Phi_k}{\partial Y}\right]\Phi_i dXdY \\ &-\xi\frac{\rho_f}{\rho_{nf}}\left[\sum_{k=1}^{N} U_k \int_\Omega \frac{\partial \Phi_i}{\partial X}\frac{\partial \Phi_k}{\partial X} dXdY + \sum_{k=1}^{N} V_k \int_\Omega \frac{\partial \Phi_i}{\partial Y}\frac{\partial \Phi_k}{\partial Y} dXdY\right] \\ &-Pr\frac{\nu_{nf}}{\nu_f}\sum_{k=1}^{N} U_k \int_\Omega \left[\frac{\partial \Phi_i}{\partial X}\frac{\partial \Phi_k}{\partial X} + \frac{\partial \Phi_i}{\partial Y}\frac{\partial \Phi_k}{\partial Y}\right] dXdY \\ &+\frac{\nu_{nf}}{Da}\int_\Omega \left(\sum_{k=1}^{N} U_k \Phi_k\right)\Phi_i dXdY \end{aligned} \tag{13}$$

$$\begin{aligned} R_i^{(2)} &= \sum_{k=1}^{N} V_k \int_\Omega \left[\left(\sum_{k=1}^{N} U_k \Phi_k\right)\frac{\partial \Phi_k}{\partial X} + \left(\sum_{k=1}^{N} V_k \Phi_k\right)\frac{\partial \Phi_k}{\partial Y}\right]\Phi_i dXdY \\ &-\xi\frac{\rho_f}{\rho_{nf}}\left[\sum_{k=1}^{N} U_k \int_\Omega \frac{\partial \Phi_i}{\partial X}\frac{\partial \Phi_k}{\partial X} dXdY + \sum_{k=1}^{N} V_k \int_\Omega \frac{\partial \Phi_i}{\partial Y}\frac{\partial \Phi_k}{\partial Y} dXdY\right] \\ &-Pr\frac{\nu_{nf}}{\nu_f}\sum_{k=1}^{N} V_k \int_\Omega \left[\frac{\partial \Phi_i}{\partial X}\frac{\partial \Phi_k}{\partial X} + \frac{\partial \Phi_i}{\partial Y}\frac{\partial \Phi_k}{\partial Y}\right] dXdY \\ &+\frac{\nu_{nf}}{Da}\int_\Omega \left(\sum_{k=1}^{N} V_k \Phi_k\right)\Phi_i dXdY \end{aligned} \tag{14}$$

$$\begin{aligned} R_i^{(3)} &= \sum_{k=1}^{N} \theta_k \int_\Omega \left[\left(\sum_{k=1}^{N} U_k \Phi_k\right)\frac{\partial \Phi_k}{\partial X} + \left(\sum_{k=1}^{N} V_k \Phi_k\right)\frac{\partial \Phi_k}{\partial Y}\right]\Phi_i dXdY \\ &-\frac{1}{Re\,Pr}\sum_{k=1}^{N} \theta_k \int_\Omega \left[\frac{\partial \Phi_i}{\partial X}\frac{\partial \Phi_k}{\partial X} + \frac{\partial \Phi_i}{\partial Y}\frac{\partial \Phi_k}{\partial Y}\right] dXdY \end{aligned} \tag{15}$$

Three points Gaussian quadrature is used to evaluate the integrals in these equations. The non-linear residual Equations (13), (14) and (15) are solved using the Newton–Raphson method to determine the coefficients of the expansions in Eq. (12). The convergence of solutions is assumed when the relative error for each variable between consecutive iterations is recorded below the convergence criterion ε such that $\left|\Psi^{n+1} - \Psi^{n}\right| \le 10^{-4}$, where n is the number of iteration and Ψ is a function of U, V and θ

4.1. Mesh Generation

In the finite element method, the mesh generation is the technique to subdivide a domain into a set of sub-domains, called finite elements, control volume etc. The discrete locations are defined by the numerical grid, at which the variables are to be calculated. It is basically a discrete representation of the geometric domain on which the problem is to be solved. The computational domains with irregular geometries by a collection of finite elements make the method a valuable practical tool for the solution of boundary value problems arising in various fields of

engineering. Fig. 2 displays the finite element mesh of the present physical domain.

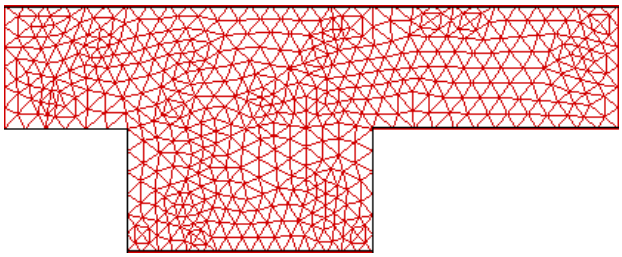

Fig. 2: Mesh generation of the channel with enclosure

4.2. Grid Independent Test

In order to determine the proper grid size for this study, a grid independence test is conducted with five types of mesh for Re = 10, Pr = 6.2, Da = 0.1 and ϕ = 5% for bottom heating case. The extreme value of Nu is used as a sensitivity measure of the accuracy of the solution and is selected as the monitoring variable. Considering both the accuracy of numerical value and computational time, the present calculations are performed with 12666 nodes and 9059 elements grid system. This is described in Table 1 and Fig. 3.

Table 2: Sensitivity Check at Re = 10, Pr = 6.2, Da = 0.1 and ϕ = 5%

Nodes (elements)	3224 (2864)	5982 (4930)	8538 (7014)	12666 (9059)	20524 (11426)
Nu	3.51465	5.40146	6.00146	6.41014	6.41015
Time (s)	259.265	392.594	488.157	521.328	727.375

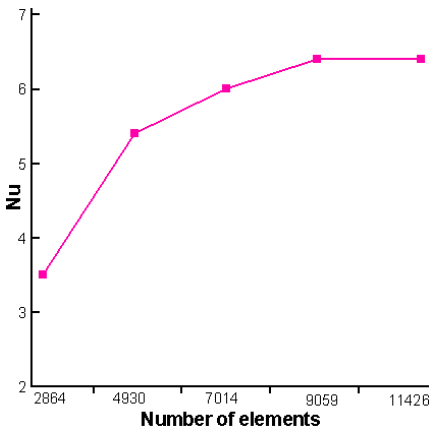

Fig. 3: Grid test for Da = 0.1, Re = 10, Pr = 6.2 and ϕ = 5%

4.3 Thermo-physical Properties

The thermo-physical properties of fluid (water) and solid TiO_2 are tabulated in Table 2. The properties are taken from [37].

Table 2. Thermo-physical properties of water-TiO_2 nanofluid

Physical properties	water	TiO_2
C_p (J/Kg K)	4179	540
ρ (Kg/m^3)	997.1	4250
K (W/m K)	0.613	8.9538
α x10^7 (m^2/s)	1.47	30.7
β (K^{-1})	2.1×10^{-4}	2.4×10^{-5}

4.4. Code Validation

The model validation is an important part of a numerical investigation. Hence, the outcome of the present numerical code is benchmarked against the numerical result of Mashaei et al. [38] which was reported for numerical investigation of nanofluid forced convection in channels with discrete heat sources. The comparison is conducted for the profile of thermal-hydraulic performance (η)-Reynolds number (Re) employing two different values of the solid volume fraction (ϕ). Fig. 4 executes an excellent agreement with Mashaei et al. [38]. This figure expresses the effect of Re and ϕ on η The validation boosts the confidence in our numerical code to carry on with the above stated objective of the current investigation.

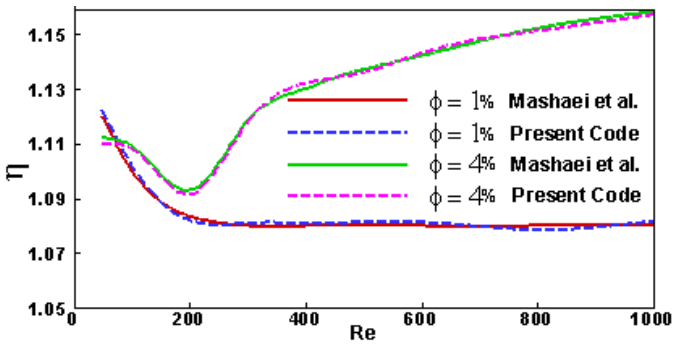

Fig. 4: Comparison of present code with Mashaei et al. [38]

In addition, the current numerical code results for the plot of maximum wall temperature $(\theta_w)_{max}$, attendant pressure drop ratio fRe/(fRe)$_0$ and Reynolds number (Re) having fixed values of Darcy number Da = 10^{-5}, dimensionless thickness of porous substrate S = 0.5 and thermal conductivity ratio R_k = 1.0 with the graphical demonstration of Sung et al. [39] which accounted forced convection from isolated heat source in a channel with

porous medium. The above declared comparison is demonstrated in the Fig. 5.

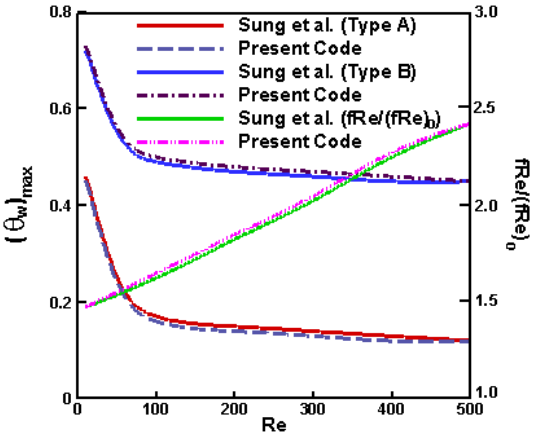

Fig. 5: Comparison between present code and Sung et al. [39] with $Da = 10^{-5}$, $S = 0.5$ and $R_k = 1.0$

5. RESULTS AND DISCUSSION

Numerical results in terms of isotherms and streamlines are displayed for various Reynolds number *Re* (= 10, 100, 200 and 300) and solid volume fraction ϕ (= 0%, 3%, 5% and 7%) while Prandtl number *Pr* = 6.2 and Darcy number *Da* = 0.1 are kept fixed. In addition, the values of the local and average Nusselt number, mean bulk temperature, mid-height horizontal and vertical velocities through the channel with an open cavity have been calculated for water titanium oxide nanofluid. In the following, several cases related to the three configurations are compared in terms of streamlines, isotherms, heat transfer rate and velocity profiles.

5.1 Effect of Reynolds number

The effects of Reynolds number *Re* on the thermal field interms of isothermal lines are presented inside the channel with left, bottom and right heated walls in Fig. 6 (i)-(iii) respectively while ϕ = 5%. We observe that as the Reynolds number enhances from 10 to 300, the temperature contours tend to get affected considerably. This figure shows that at low values of *Re*, the temperature of the nanofluid rapidly reaches to the temperature of heated (by uniform heat flux) walls due to low viscosity. With increasing Reynolds number, decrement of temperature of water-TiO_2 nonofluid happens slowly which leads to increment of peaks of isothermal lines at the exit port of the channel. Rising *Re* leads to formation of the thermal boundary layer at the heated surfaces. This means that higher heat transfer rate is predicted by the working water- TiO_2 nanofluid. Isotherms become compressed in a zone close to the hot walls of the open cavity for higher values of *Re*. Because increasing *Re* causes more flow of the working nanofluid. Then the average heat transfer enhances by utilizing water-TiO_2 nanofluid along the channel with an open cavity.

On the other hand influences of Reynolds number *Re* on the velocity field are presented inside the channel with left, bottom and right heated walls in Fig. 7 (i)-(iii) respectively. In the form of streamlines we represent the velocity (modulus of the velocity vector) field. As the Rayleigh number decreases, as shown in Fig. 7, the intensity of the main circulation decreases and fills the entire enclosure. In the velocity vector, initially the flow covers the whole domain of the channel with an open cavity while it goes up from the bottom surface of the cavity and tends to gather to the middle of the channel due to increase inertia force from 10 to 300. Thus there creates an empty space near the bottom surface of the cavity.

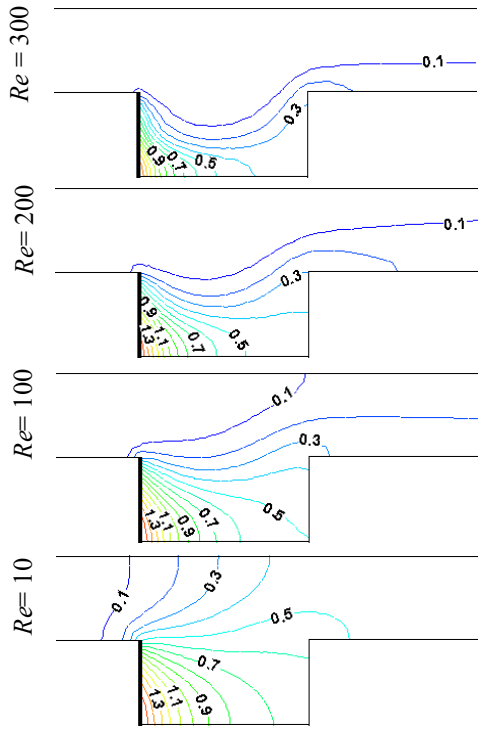

6 (i)

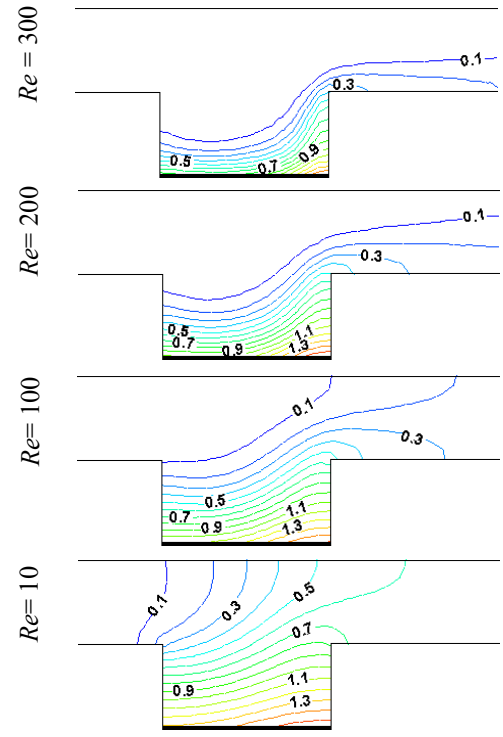

6 (ii)

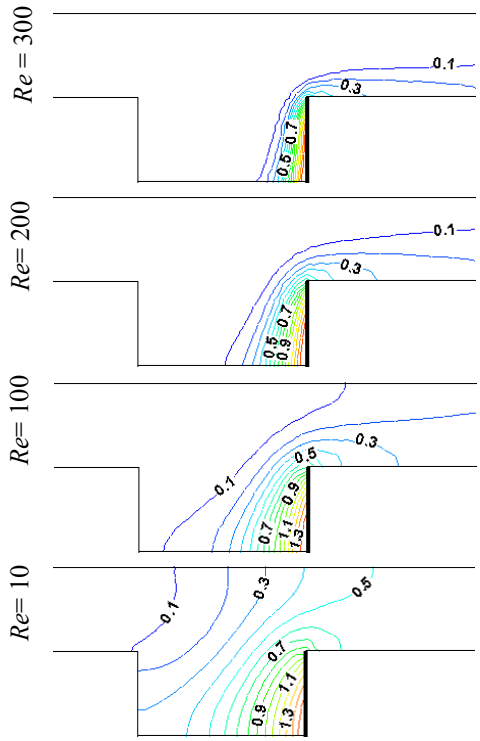

6 (iii)

Fig. 6: Effect of *Re* on isothermal lines for (i) left (ii) bottom and (iii) right heating walls at $\phi = 5\%$

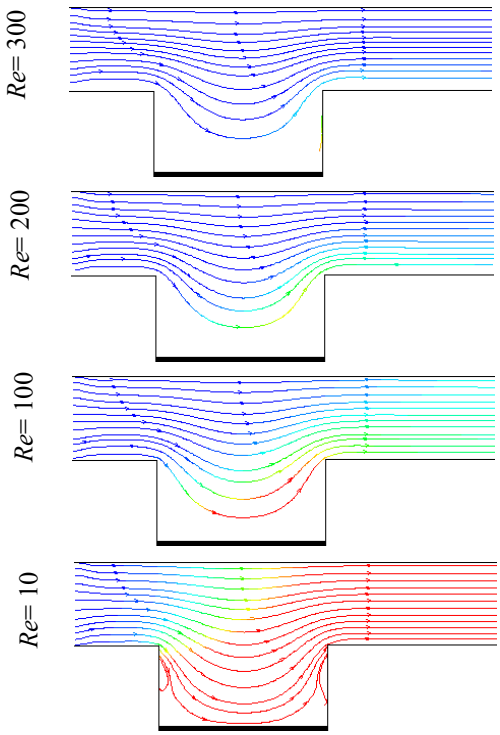

7 (ii)

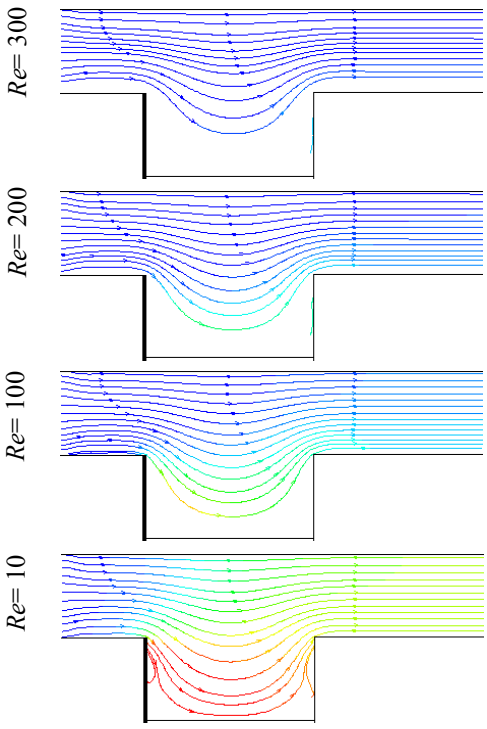

7 (i)

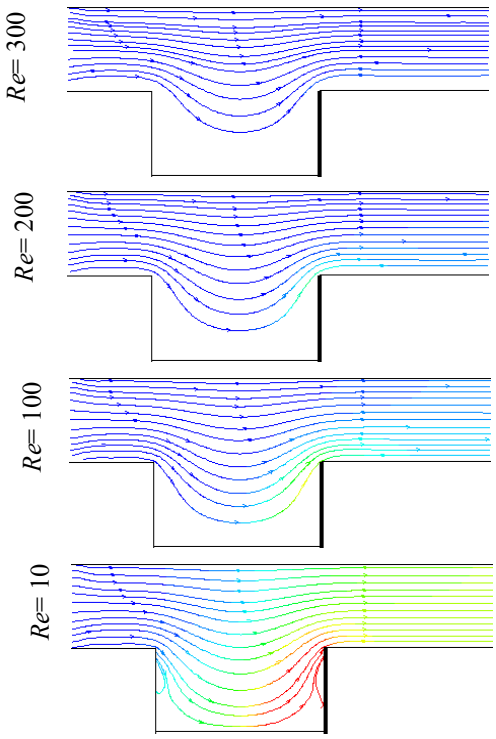

7 (iii)

Fig. 7: Effect of *Re* on streamlines for (i)left, (ii) bottom and (iii) right heating walls at $\phi = 5\%$

5.2 Effect of solid volume fraction

Fig. 8 (i) – (iii) shows the influences of solid volume fraction (ϕ) on the temperature profile while Re = 10. The strength of the thermal current activities is more activated with escalating ϕ from 0% (clear water) to 7%. The temperature lines through the horizontal pipe with an open cavity dense near the inlet for increasing ϕ. But initially (ϕ = 0%) these lines try to gather near the heated walls of the cavity corresponding to physical changes of the working fluid. Increasing solid volume fraction causes the enhancement of thermal conductivity of the nanofluid. Due to rising values of ϕ, the temperature distributions become distorted resulting in an increase in the overall heat transfer. This result can be attributed to the performance of the solid volume fraction. It is worth noting that as the ϕ increases, the thickness of the thermal boundary layer near the input opening enhances which indicates a steep temperature gradient and hence, an increase in the overall heat transfer through the channel with an open cavity.

Fig. 9 (i)-(iii) shows that there is no significant change in the streamlines except the middle part of the channel. At first the flow concentrates near the middle horizontal part of the channel while it covers the whole domain of the channel due to increase solid volume fraction from 0% to 7%. This is due to the fact that base fluid (ϕ = 0%) moves rapidly than solid concentrated water-TiO_2 nanofluid. Fig. 9 (ii) describes the heating from below where the streamlines are very similar to those reported in Fig. 9(i) and (iii) because the solid volume effect is overwhelmed by the effect of the inertia force. The streamlines have very low velocity values in the zone adjacent the bottom heated wall for higher values of solid concentration.

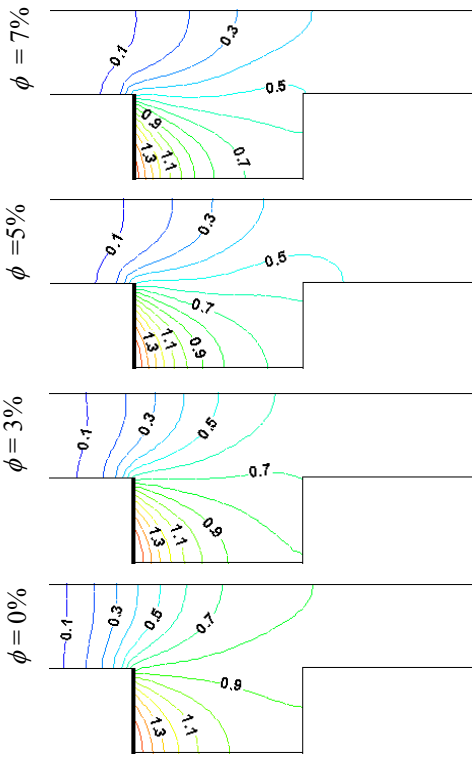

8 (i)

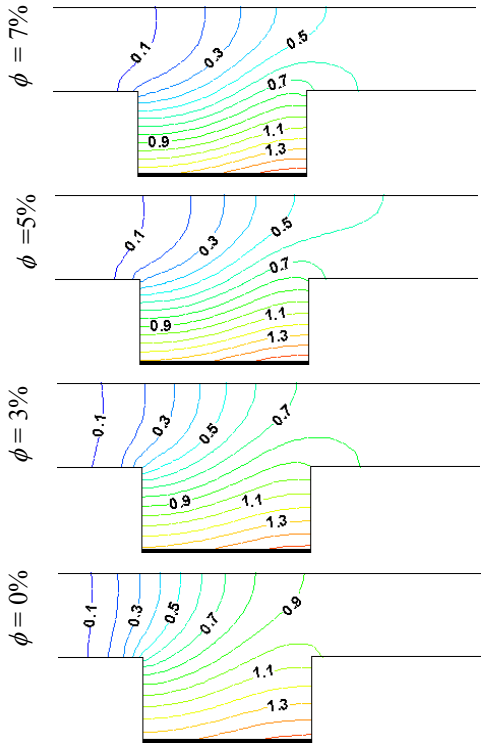

8 (ii)

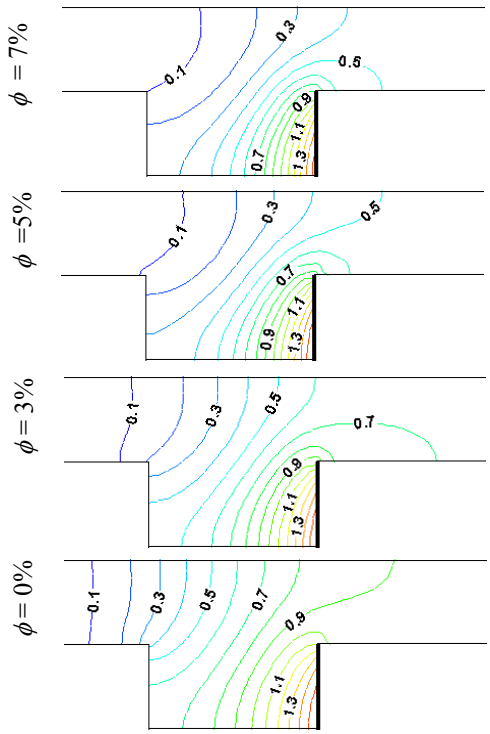

8 (iii)

Fig. 8: Effect of ϕ on isothermal lines for (i) left, (ii) bottom and (iii) right heating walls at Re = 10

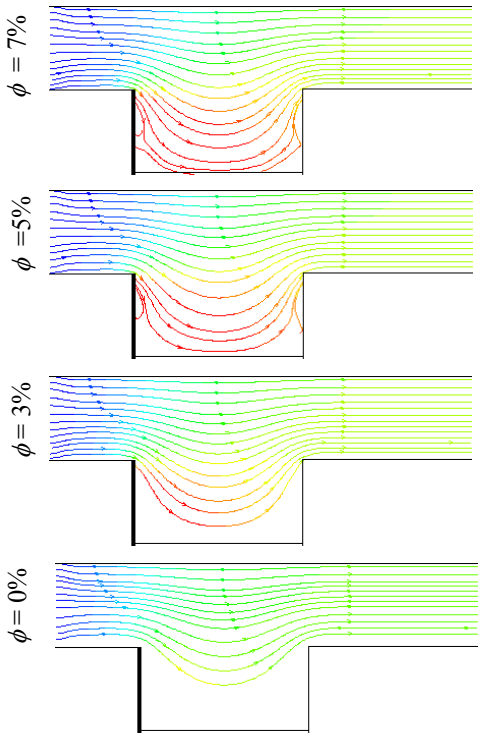

9 (i)

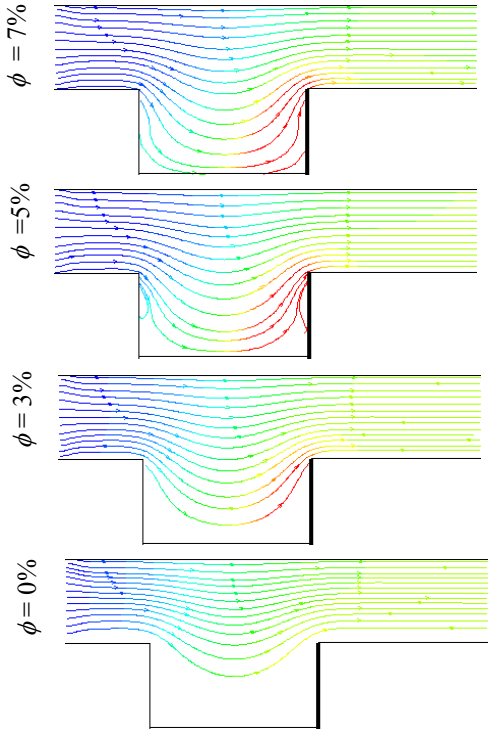

9 (iii)

Fig. 9: Effect of ϕ on streamlines for (i)left, (ii) bottom and (iii) right heating walls at Re = 10

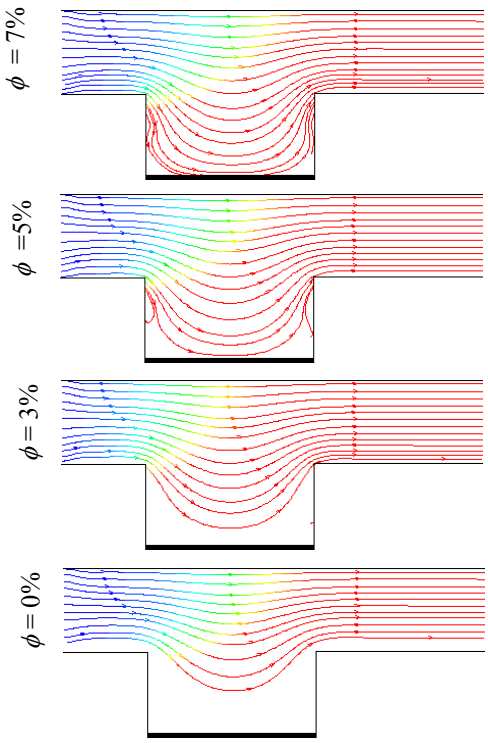

9 (ii)

5.3 Local Nusselt number

A plot of the local Nusselt number (Nu_{local}) along the bottom heated wall of the cavity for different Re and ϕ is expressed in Fig. 10(i)-(iii) and 11(i)-(iii). The shape of $Nu_{local} - Y$ (0 - 0.1) profile for assisting flow and $Nu_{local} - X$ (0.1 - 0.3) profile for bottom heating are parabolic. But some discrepancies are observed in $Nu_{local} - Y$ (0 - 0.1) profile for opposing flow. Local heat transfer increases for rising both the parameters namely Reynolds number Re and solid volume fraction ϕ of the water-TiO_2 nanofluid.

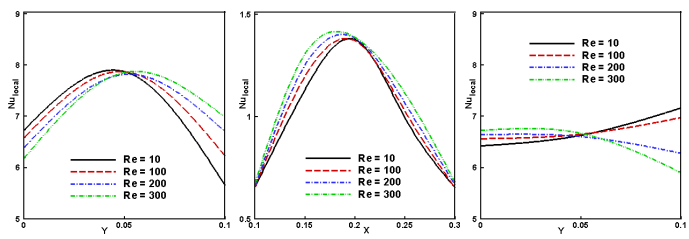

(i) **(ii)** **(iii)**

Fig. 10: local Nusselt number for the effect of Re with (i) left, (ii) bottom and (iii) right heated wall

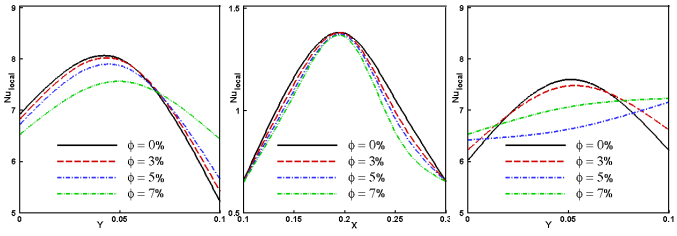

(i) **(ii)** **(iii)**

Fig. 11: local Nusselt number for the effect of ϕ with (i) left, (ii) bottom and (iii) right heated wall

5.4 Mean Nusselt number

Fig. 12 (i)-(ii) depicts the mean Nusselt number (*Nu*) with the variation of *Re* and ϕ. In this figure we consider heat transfer rate as a function of Reynolds number (*Re*) as well as solid volume fraction (ϕ). We consider the values of Reynolds number are 10, 100, 200 and 300. From *Nu*-*Re* profiles it is clearly shown that escalating *Re* and ϕ lead the enhancement of heat transfer rate. Maximum heat transfer rate is observed for opposing flow for both parameters. Rate of heat transfer rises by 11%, 12% and 14% for assisting flow, heating from below and opposing flow respectively with the effect of *Re*. For assisting flow, heating from below and opposing flow the heat transfer rate increases by 7%, 10% and 12% respectively with the influence of ϕ.

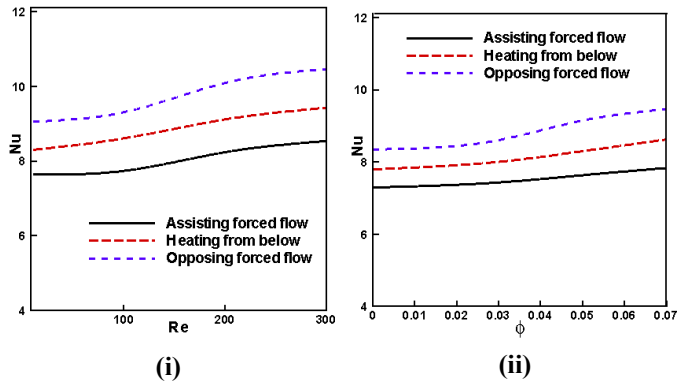

(i) **(ii)**

Fig. 12: Average Nusselt number for the effect of (i) *Re* and (ii) ϕ

5.5 Average temperature

The mean bulk non-dimensional temperature (θ_{av}) of the nanofluid inside the channel with an open cavity for the effect of *Re* and ϕ are displayed in Fig. 13 (i)-(ii). θ_{av} devalues for escalating *Re*. Rising inertia force causes the reduction of fluid temperature. On the other hand, average temperature of the fluid grows up with the variation of ϕ. This is due to the fact that the thermal conductivity of nanofluid is always higher than base fluid (ϕ = 0%). Higher thermal conductivity of the water-titanium oxide nanofluid can carry more heat. For opposing forced flow, the non-dimensional temperature of the working nanofluid is higher than the other flows (the assisting flow and heating from below).

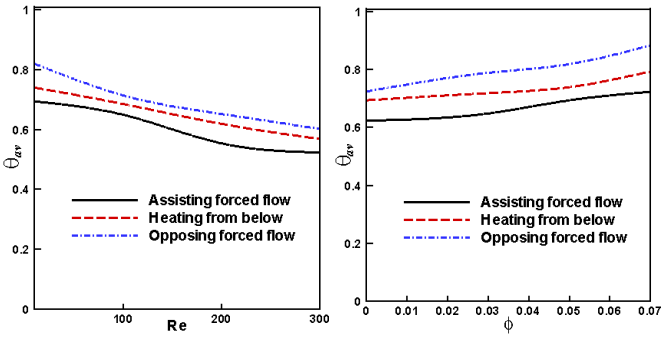

(i) **(ii)**

Fig. 13: Mean temperature for the effect of (i) *Re* and (ii) ϕ

5.6 Mid height horizontal velocity

Figs. 14 (i)-(iii) and 15 (i)-(iii) display the mid height horizontal (*U*) velocity at $X = 0.2$ for various Reynolds number and solid volume fraction respectively. It is seen from these figures that the waviness of the *U* velocity profile for the considered highest Reynolds number (*Re* = 300) and lowest solid volume fraction (ϕ = 0%) is found greater than the remaining values of these two parameters. This happens because the decrease of inertia force and increase of solid concentration in nanofluid lead to retardation in the velocity profile inside the channel. For both parameters opposing flow introduces more perturbation in the *U*-*Y* velocity profile among other configurations of heating by uniformly heat flux.

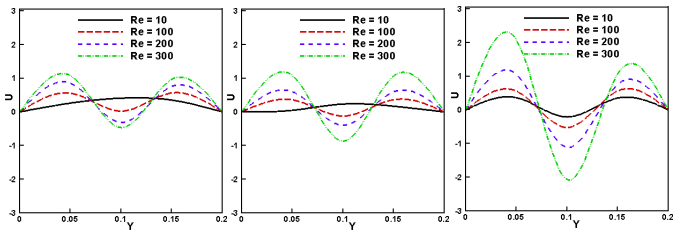

(i) **(ii)** **(iii)**

Fig. 14: Mid height *U*-velocity for the effect of *Re* with (i) left, (ii) bottom and (iii) right heated walls

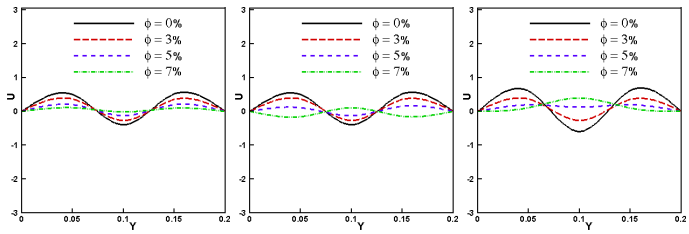

(i) **(ii)** **(iii)**

Fig. 15: Mid height horizontal velocity for the effect of ϕ with (i) left, (ii) bottom and (iii) right heated walls

5.7 Mid height vertical velocity

The plots of mid height vertical (V) velocity at Y = 0.15 of the nanofluid through the channel for the influences of Re and ϕ are exposed graphically in Figs. 16(i)-(iii) and 17 (i)-(iii) respectively. A remarkable change is seen in the V-X profile with applying inertia force of the water-TiO_2 nanofluid. The vertical velocity component devalues with mounting solid volume fraction. It is desired that, clear water moves more rapidly than the solid concentrated nanofluid. No remarkable change is found in the pattern of V-X velocity profile due to changing heating locations. In the case of opposing flow, minor variation is seen in the velocity graph for both parameters.

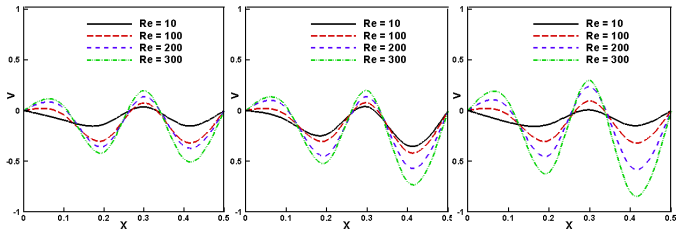

Fig. 16: Mid height V-velocity for the effect of ϕ with (i) left, (ii) bottom and (iii) right heated walls

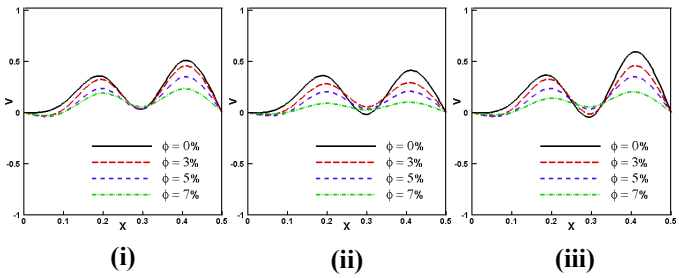

Fig. 17: local Nusselt number for the effect of ϕ with (i) left, (ii) bottom and (iii) right heated wall

5.8 Normalized Nusselt number

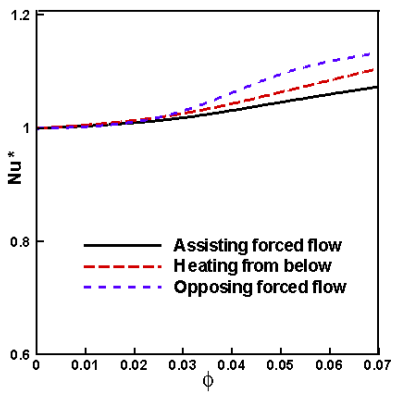

Fig. 18: Normalized Nusselt number

The design of normalized Nusselt number (Nu*) for the effect of solid volume fraction ϕ is represented in Fig. 18. Nu* grows with the variation of solid volume fraction for the water based TiO_2 nanofluid. Opposing flow causes the highest value of normalized Nusselt number.

6. CONCLUSION

The effect of heating wall position on assisted (forced) convection heat transfer in a horizontal channel with an open cavity filled with water-TiO_2 nanofluid has been studied numerically. The results are showed for three different heating modes with the variation of Reynolds number and solid volume fraction. Temperature and flow field in terms of isotherms and streamlines have been displayed. The results of the current numerical analysis lead to the following conclusions:

- The structure of the fluid flow and temperature field through the channel is found to be significantly dependent upon the Reynolds number and solid volume fraction.
- Escalating Re and ϕ improve the heat removal from the heat source for the opposing flow case.
- There is a considerable change in the distribution of local Nusselt number.
- The maximum rate of heat transfer is obtained for the opposing flow with the highest value of both Re and ϕ.
- The mean temperature of the fluid in the channel decrease with rising Re and lessening ϕ.
- The mid height horizontal and vertical velocities are perturbed appreciably for the case of opposing flow among the considered three heating locations.

7. REFERENCES

[1] A. Cabal, J. Szumbarski, JM. Floryan, Stability of flow in a wavy channel, J. Fluid Mech., Vol. 457, pp. 191–212, 2002.

[2] SM. Aminossadati, B. Ghasemi, A numerical study of mixed convection in a horizontal channel with a discrete heat source in an open cavity, European J. of Mechanics B-Fluids, Vol. 28, No. 4, pp. 590-598, 2009.

[3] S. Mahmud, AKMS. Islam, MAH. Mamun, Separation characteristics of fluid flow inside two parallel plates with wavy surface, Int. J. Eng. Sci., Vol. 40, pp. 1495–1509, 2002.

[4] S. Mahmud, AKMS. Islam, CM. Feroz, Flow and heat transfer characteristics inside a wavy tube, Heat Mass Transfer, Vol. 39, pp. 387–393, 2003.

[5] O. Manca and S. Nardini, K. Khanafer and K. Vafai, Effect of heated wall position on mixed convection in a channel with an open cavity, Num. Heat Trans., Part A, Vol. 43, pp. 259–282, 2003.

[6] L. Adjlout, O. Imine, A. Azzi, M. Belkadi, Laminar natural convection in an inclined cavity with a wavy wall, Int. J. Heat Mass Trans., Vol. 45, pp. 2141–2152, 2002.

[7] PK. Das, S. Mahmud, Numerical investigation of natural convection in a wavy enclosure, Int. J. Therm. Sci., vol. 42, pp. 397–406, 2003.

[8] S. Mahmud, AKMS. Islam, Natural convection and entropy generation in an inclined wavy enclosure, Int. J. Therm. Sci., Vol. 42, pp. 1003–1012, 2003.

[9] BVR. Kumar, A study of free convection induced by a vertical wavy surface with heat flux in a porous enclosure, Numer. Heat Trans., Part A, Vol. 37, pp. 493–510, 2000.

[10] BVR. Kumar, S. Gupta, Free convection in a non-Darcian wavy porous enclosure, Int. J. Eng. Sci., Vol. 41, pp. 1827–1848, 2003.

[11] BVR. Kumar, S. Gupta, Free convection in a thermally stratified non-Darcian wavy enclosure, J. Porous Media, Vol. 7, pp. 261–277, 2004.

[12] A. Misirlioglu, AC. Baytas, I. Pop, Free convection in a wavy cavity filled with a porous medium, Int. J. Heat Mass Trans., Vol. 48, pp. 1840–1850, 2005.

[13] AK. Santra, S. Sen, N. Chakraborty, Study of heat transfer characteristics of copper–water nanofluid in a differentially heated square cavity with different viscosity models, J. of Enhanced Heat Trans., Vol. 15, No. 4, pp. 273-287, 2008.

[14] S. Kumar, SK. Prasad, J. Banerjee, Analysis of flow and thermal field in nanofluid using a single phase thermal dispersion model, Appl. Mathematical Modelling, Vol. 34, pp. 573–592, 2009.

[15] B. Ghasemi, SM. Aminossadati, Natural convection heat transfer in an inclined enclosure filled with a water–CuO nanofluid, Numerical Heat Trans., Part A, Vol. 55, pp. 807-823, 2009.

[16] E. Abu-Nada, HF. Oztop, Effects of inclination angle on natural convection in enclosures filled with Cu–water nanofluid, Int. J. for Heat & Fluid Flow, Vol. 30, pp. 669-678, 2009.

[17] M. Muthtamilselvan, P. Kandaswamy, J. Lee, Heat transfer enhancement of copper–water nanofluids in a lid-driven enclosure, Commun. in Nonlinear Sci. and Num. Simulation, Vol. 15, No. 6, pp. 1501-1510, 2009.

[18] E. Abu-Nada, Z. Masoud, HF. Oztop, A. Campo, Effect of nanofluid variable properties on natural convection in enclosures, Int. J. of Thermal Sci., Vol. 49, pp. 479-491, 2010.

[19] X. Chen, JM. Li, WT. Dai and BX. Wang, Enhancing convection heat transfer in mini tubes with nanoparticle suspensions, J. Eng. Thermophys., Vol. 25, No. 4, pp. 643-645, 2004.

[20] WT. Dai, JM. Li, X. Chen and BX. Wang, Experimental investigation on convective heat transfer of copper oxide nonoparticle suspensions inside mini-diameter tubes, J. Eng. Thermophys., Vol. 24, No. 4, pp. 633-636, 2003.

[21] E. Pfautsch, Forced convection in nanofluids over a flat plate, Thesis Presented to the Faculty of the Graduate School, University of Missouri, 2008.

[22] R. Nasrin, S. Parvin, MA. Alim and AJ. Chamkha, Non-darcy forced convection through a wavy channel using CuO nanofluid, Int. J. of Energy & Tech., Vol. 4, No. 8, pp. 1-8, 2012.

[23] M. Yang, R. Yeh, J. Hwang, Forced convection in a channel with transverse fins, Int. J. of Num. Methods for Heat and Fluid Flow, Vol. 22, No. 3, pp. 306 – 322, 2012.

[24] R. Nasrin, S. Parvin, M.A. Alim and A.J. Chamkha, Transient analysis on forced convection phenomena in a fluid valve using nanofluid, Num. Heat Trans., Part A-Applications, Vol. 62, No. 7, pp. 589 – 604, 2012.

[25] M. Sathiyamoorthy, A.J. Chamkha, Natural convection flow under magnetic field in a square cavity for uniformly (or) linearly heated adjacent walls, Int. J. of Num. Meth. for Heat and Fluid Flow, Vol. 22, No. 5, pp. 677 – 698, 2012.

[26] R. Nasrin, M.A. Alim and A.J. Chamkha, Modeling of mixed convective heat transfer utilizing nanofluid in a double lid driven chamber with internal heat generation, Int. J. of Num. Meth. for Heat and Fluid Flow (Accepted).

[27] R. Nasrin, Rayleigh and Prandtl number effects on free and forced magnetoconvection in a lid driven enclosure with wavy bottom wall, Int. J. of Energy and Tech., Vol. 3, No. 23, pp.1-8, 2011.

[28] R. Nasrin and MA. Alim, Effect of nanoparticle volume fraction on buoyant flow in a solar collector with undulating absorber, Int. J. of Energy & Tech., Vol. 4, No. 19, pp. 1-9, 2012.

[29] R Nasrin, S. Parvin, M.A. Alim and A.J. Chamkha, Non-darcy forced convection through a wavy channel using CuO nanofluid, Int. J. of Energy & Tech., Vol. 4, No. 8, pp. 1-8, 2012.

[30] R Nasrin, and M.A. Alim, Dufour-Soret effects on natural convection inside a solar collector utilizing water-cuo nanofluid, Int. J. of Energy & Tech., Vol. 4, No. 23, pp. 1-10, 2012.

[31] R. Nasrin and MA. Alim, Analysis of physical parameters on forced convection along a horizontal corrugated pipe with nanofluid, Engg. e- Transaction, Vol. 7, No. 1, pp. 14-22, 2012.

[32] N. Guerroudj, H. Kahalerras, Mixed convection in an inclined channel with heated porous blocks, Int. J. of Num. Meth. for Heat and Fluid Flow, Vol. 22, No. 7, pp. 839 – 861, 2012.

[33] BC. Pak, Y. Cho, Hydrodynamic and heat transfer study of dispersed fluids with submicron metallic oxide particle, Experimental Heat Trans., Vol.11, pp.151-170, 1998.

[34] JC. Maxwell-Garnett, Colours in metal glasses and in metallic films, Philos. Trans. Roy. Soc. A, Vol. 203, pp. 385–420, 1904.

[35] C. Taylor, P. Hood, A numerical solution of the Navier-Stokes equations using finite element technique, Computer and Fluids, Vol. 1, pp. 73-89, 1973.

[36] P. Dechaumphai, Finite Element Method in Engineering, 2nd ed., Chulalongkorn University Press, Bangkok, 1999.

[37] EB. Ogut, Natural convection of water-based nanofluids in an inclined enclosure with a heat source, Int. J. of Thermal Sci., Vol. 48, No. 11, pp. 2063-2073, 2009.

[38] PR. Mashaei, SM. Hosseinalipour and M. Bahiraei, Numerical investigation of nanofluid forced convection in channels with discrete heat sources, J. of Appl. Mathematics, Vol. 2012 (2012), Article ID 259284, 18 pages, doi:10.1155/2012/259284, 2012.

[39] HJ. Sung, SY. Kim, and JM. Hyun, Forced convection from isolated heat source in a channel with porous medium, Int. J. of Heat and Fluid Flow, Vol.16, pp. 527-535, 1995.

NOMENCLATURE

C_p	Specific heat at constant pressure (kJ kg^{-1} K^{-1})
Da	Darcy number, $Da = \dfrac{K}{H^2}$
H	Dimensional height of channel (m)
k	Thermal conductivity (W m^{-1} K^{-1})
L	Dimensionless length of the heated wall
Nu	Nusselt number
p	Dimensional pressure (Kg m^{-1} s^{-2})
P	Non-dimensional pressure, $P = \dfrac{p}{\rho_f U_i^{\,2}}$
Pr	Prandtl number, $Pr = \nu_f / \alpha_f$
q	Heat flux, (W m^{-2})
Re	Reynolds number, $Re = \dfrac{U_i H}{\nu_f}$
T	Dimensional temperature (^{o}K)
u, v	Dimensional velocity components (m s^{-1})
U, V	Dimensionless velocities, $U = u/U_i$, $V = v/U_i$
X, Y	Dimensionless coordinates, $X = x/H$, $Y = y/H$
x, y	Dimensional coordinates (m)

Greek Symbols

α	Fluid thermal diffusivity (m^2 s^{-1})
β	Thermal expansion coefficient (K^{-1})
ϕ	Nanoparticles volume fraction
ν	Kinematic viscosity (m^2 s^{-1})
θ	Dimensionless temperature, $\theta = (T - T_i) k_f / qH$
ρ	Density (kg m^{-3})
μ	Dynamic viscosity (N s m^{-2})

Subscripts

av	average
f	fluid
i	inlet state
nf	nanofluid
s	solid particle